Geometries, Stabilities, and Growth Patterns of the Bimetal Mo_2-doped Si_n ($n = 9-16$) Clusters: A Density Functional Investigation

Ju-Guang Han,*,† Run-Ning Zhao,‡ and Yuhua Duan§

Department of Chemistry and Biochemistry, Montana State University, Bozeman, Montana 59717, Institute of Photonics & Photon-Technology, Northwest University, Xi'an 710069, People's Republic of China, U.S. Department of Energy, National Energy Technology Laboratory, Pittsburgh, Pennsylvania 15236, and Parsons Project Services Inc., South Park, Pennsylvania 15129

Received: September 21, 2006; In Final Form: January 6, 2007

The behaviors of the bimetal Mo−Mo doped cagelike silicon clusters Mo_2Si_n at the size of $n = 9-16$ have been investigated systematically with the density functional approach. The growth-pattern behaviors, relative stabilities, and charge-transfer of these clusters are presented and discussed. The optimized geometries reveal that the dominant growth patterns of the bimetal Mo−Mo doped on opened cagelike silicon clusters ($n = 9-13$) are based on pentagon prism $MoSi_{10}$ and hexagonal prism $MoSi_{12}$ clusters, while the Mo_2 encapsulated Si_n($n = 14-16$) frames are dominant growth behaviors for the large-sized clusters. The doped Mo_2 dimer in the Si_n frames is dissociated under the interactions of the Mo_2 and Si_n frames which are examined in term of the calculated Mo−Mo distance. The calculated fragmentation energies manifest that the remarkable local maximums of stable clusters are Mo_2-doped Si_n with $n = 10$ and 12; the obtained relative stabilities exhibit that the Mo_2-doped Si_{10} cluster is the most stable species in all different sized clusters. Natural population analysis shows that the charge-transfer phenomena appearing in the Mo_2-doped Si_n clusters are analogous to the single transition metal Re or W doped silicon clusters. In addition, the properties of frontier orbitals of Mo_2-doped Si_n ($n = 10$ and 12) clusters show that the Mo_2Si_{10} and Mo_2Si_{12} isomers have enhanced chemical stabilities because of their larger HOMO−LUMO gaps. Interestingly, the geometry of the most stable Mo_2Si_9 cluster has the framework which is analogous to that of Ni_2Ge_9 cluster confirmed by recent experimental observation (Goicoechea, J. M.; Sevov, S. C. *J. Am Chem. Soc*. **2006**, *128*, 4155).

1. Introduction

Silicon and germanium clusters have been studied extensively by both theoretical and experimental techniques because they may be employed as the building blocks for developing new silicon-based nanomaterials with tunable properties.[1−21] After the transition metal (TM) is doped into the silicon frame, the TM doped silicon clusters exhibit a variety of geometrical arrangement and electronic properties,[21−34] tend to form closed-shell electronic structures that show the extraordinary stabilities comparing with the pure species, and contribute to generating novel transition metal encapsulated clusters with novel properties.

In a pioneering series of experimental measurements, Beck[18] generated mixed transition metal silicide clusters of composition $TM@Si_nH_x$ (TM═Cu, Mo, W) by laser vaporization supersonic expansion technique. These cluster units were found to be more stable toward photofragmentation than pure Si_n clusters of similar size. Scherer et al.[12] produced mixed transition metal silicides by time-of-flight mass spectroscopy and studied the electronic states of CuSi, AgSi, and AuSi dimers by measuring their laser absorption spectra. In addition, the VSi and NbSi dimers have been investigated by matrix-isolated ESP spectroscopy.[5] Recently, the previous works on the stable $TMSi_n$ (TM═Cr, Mo, W, Hf, Ta, W, Re, Ir; $n = 14, 13, 12, 11, 9$)[19] and $TbSi_n^-$ ($6 \le n \le 16$)[22] were studied experimentally by aid of various technical methods. The photoelectron spectra of the chromium-doped silicon cluster anions, $CrSi_n^-$ ($n = 8-12$),[21] were measured. From the measurements of vertical detachment energies, enhanced stability was found for the unit $CrSi_{12}$. The experimental results on vertical detachment energies indicate that the $CrSi_{12}$ unit has enhanced stability with chromium atom being encapsulated inside the Si_{12} cage.[21]

Stimulated by these experiment observations, many computational investigations have been performed for one transition metal doped silicon clusters.[22−35] Although the mixed Cu_mSi_n clusters were detected by mass spectroscopy experimentally,[20] to our knowledge, no detailed theoretical investigations on the mixed transition metals TM_n ($n > 1$) doped silicon clusters have been performed until now. In order to reveal the unusual properties of the bimetal Mo_2-doped silicon clusters, the main objective of this research, therefore, is to provide a detailed investigation of the equilibrium geometries, relative stabilities, fragmentation energies [$D(n,n-1)$], the atomic averaged binding energies [$E_b(n)$], charge transfer of the Mo_2Si_n clusters, and to explore the growth-pattern mechanisms of the polymetal doped silicon clusters, which can provide significant help in the quest for such kind of cluster assembled materials.

2. Computational Details

In order to provide the accurate and reliable results, we carry out the detailed density functional theory (DFT) investigation

* To whom correspondence should be addressed. E-mail: jghan@ustc.edu.cn.
† Montana State University.
‡ Northwest University.
§ U.S. Department of Energy and Parsons Project Services Inc.

10.1021/jp0661903 CCC: $37.00
Published on Web 02/23/2007

TABLE 1: The Calculated Bond Length Dissociation Energy, Frequency, and Electronic State for the Si_2, Mo_2, and MoSi Clusters

clusters	method	bond length(Å)	dissociation energy(eV)	frequency (cm^{-1})	electronic state
Si_2	B3LYP	2.35	2.62	445.7	$^3\Sigma^-_g$
	EXP[a]	2.25	3.22	511.0	$^3\Sigma^-_g$
	ADF[b]	2.31	3.30	463.5	$^3\Sigma^-_g$
Mo_2	B3LYP	1.98	1.75	562.0	$^1\Sigma^+_g$
	LSDA[c]	1.95	2.17	520.0	$^1\Sigma^+_g$
	EXP[d]	1.94	2.19	477.0	$^1\Sigma^+_g$
MoSi	B3LYP	2.40	1.90	316.6	$^5\Pi$
	B3LYP[e]	2.36	2.08		$^5\Pi$

[a] Ref 40. [b] Ref 29. [c] Ref 44. [d] Ref 45. [e] Ref 24.

on the Mo−Mo doped silicon clusters at the size range ($9 \le n \le 16$). The equilibrium geometries and electronic properties of the Mo_2 doped silicon clusters are performed by DFT with the unrestricted B3LYP exchange-correlation potential[36,37] and an effective core potential LanL2DZ basis sets. The standard LanL2DZ basis sets[38] are employed to provide an effective way to reduce difficulties in calculations of two-electron integrals caused by heavy transition metal Mo atoms. All computational works are carried out by Gaussian 03 package.[39] The polarization basis sets are not considered in this work because our previous work[32] showed that they are insignificant to our results. Here is the more information about what structures should be considered for our clusters. It should be pointed out that a small number of structures were tried for each size n, and that these structures were taken from prior studies of singly-TM doped Si_n clusters.[3,8,11,14,25−32] For clusters containing 12−18 atoms, as considered here, there are a very large number of local minima for each size, and it is in no way obvious that the small subset chosen contains the best structures. Therefore, in this study we try to examine if the localization of Mo atoms upon/into silicon clusters changes the major rearrangement of the geometry framework of Si_n clusters (or cages) as well as to reveal the striking change in properties due to the inserting of the various metals. Fortunately, previous theoretical results on MSi_n (M═W and Re) and MGe_n (M═W, Cu, and Ni) are available[3,8,11,14,25−32] and can be considered into our structure optimization. For each stationary point of a cluster, the stability is reassured by the calculated harmonic vibrational frequencies. If the unstable geometry with one imaginary frequency is found, a relaxation along the coordinates of the imaginary vibrational mode is rearranged until a true local minimum is finally reached. Therefore, geometries and total energies for each stable cluster and its stable isomers actually correspond to the local minima. As the number of isomers is increased quickly with the cluster size, it is very difficult to obtain the global minimum simply according to the calculated total energies of the isomers.

In order to obtain the most possible stable Mo_2Si_n ($n = 9-16$) clusters, some previous available theoretical or experimental results are considered first, then the equilibrium geometry is determined by varying the geometry starting from high-symmetry structure to low-symmetry structure. This leads to a limited number of possible stable structures for each size of cluster.

To test the reliability of our calculations, the Si_2, Mo_2, and MoSi molecules are carried out, and the calculated bond lengths, vibrational frequencies, and dissociation energies are illustrated in Table 1. From Table 1, one can find that the calculated results of the Si_2, Mo_2, and MoSi clusters are in good agreement with the reported theoretical and experimental results that are available.[24,40−44] This examination of equilibrium bond lengths and angles leads to deviations typically within 1−6%. Since the calculated results also depend on the pseudopotentials, our study can be considered as preliminary and qualitative in nature. On the basis of the calculated results, it should be pointed out that the dissociation energy of the MoSi cluster is smaller than that of the Si_2 cluster, but bigger than that in the free Mo_2 molecule. This result reflects that in the Mo_2Si_n clusters the Si−Si interaction is stronger than the Mo−Si and Mo−Mo interactions and plays a dominant role in stabilizing the Mo_2-Si_n clusters.

3. Results and Discussions

3.1. Geometries and Stabilities. Mo_2Si_9. Considering of all the possible geometries, three stable isomers have been identified for the Mo_2Si_9 cluster as shown in Figure 1. On the basis of the calculated total energies, which are listed in Table 2, we find that the 9a isomer is slightly higher in total energy than the 9b isomer does; therefore, the 9b isomer is more stable than the 9a isomer. Interestingly, structure 9a and structure 9b have different equilibrium geometries and can be considered as the degenerated isomers with different framework of silicon clusters because the energetic difference between these two isomers is very small. In addition, both 9a and 9b isomers can be described as one Mo atom being surface capped on the $MoSi_9$ frame after other Mo atom being encapsulated into the Si_9 frame. With respect to the 9c isomer, the optimized equilibrium geometry has the frame which is analogous to the experimental structure of the Ni_2Ge_9 cluster[33] and can be described as one Mo being surface capped on the antiprism $MoSi_9$ frame. However, the total energy of the 9c isomer is distinctly higher than that of the 9a and 9b isomers, which indicates that the 9c isomer is less stable than the 9a and 9b isomers. Consequently, the 9b isomer with the encapsulated Mo atom having tendency to terminate the dangling bonds of the Si_9 frame and trying to interact with all silicon atoms directly with unequivalent bond lengths is selected as the most stable isomer and the ground state for cluster Mo_2Si_9. In addition, from our optimization the most stable Mo_2Si_9 9b geometry is different from the experimental geometry of the Ni_2Ge_9 cluster.[33]

Mo_2Si_{10}. Four possible geometries of the Mo_2Si_{10} cluster (Figure 1), which are described as the pentagonal antiprism C_s Mo_2Si_{10} 10a, two pyramidal Si_4 capped rhombus Mo_2Si_2 C_s 10b, the Mo surface capped sandwich-like prism C_1 $MoSi_{10}$ 10c, and the two separated Si atoms surface capped planar Mo_2Si_8 isomer 10d, are optimized, together with the harmonic frequency analysis. The pentagonal antiprism Mo_2Si_{10} 10a isomer can be seen as the Mo_2 atoms being vertically doped in the pentagonal antiprism Si_{10} frame. Interestingly, the two Mo_2 atoms in the Mo_2Si_{10} are bonded together with bond distance of 2.322 Å, which is longer than that (1.975 Å) of the Mo_2 dimer; this result indicates that the Mo−Mo bond is elongated after it is inserted into the Si_{10} frame due to the interactions among the Mo atoms and Si frame resulting from the charge-transfer which will be discussed below. The C_s 10b isomer is described as the Mo_2 being parallel doped the two pyramidal Si_4 frames. The Mo−Mo bond length in the 10b isomer is longer than that in the 10a isomer, and the C_s 10b isomer is more stable than C_s 10a isomer because the total energy of 10b isomer is lower by 1.026 eV than that of 10a isomer. As for as the C_1 10c isomer is concerned, it is depicted as one Mo being surface capped on the bipentagonal prism $MoSi_{10}$ frame; however, the Mo−Mo bond length in the 10c isomer is longer than that in the 10a and 10b isomers, and the total energy of the 10c isomer is lower than those of the 10a and 10b isomers by 1.851 and 0.825 eV, respectively. From our calculated total energies shown in Table

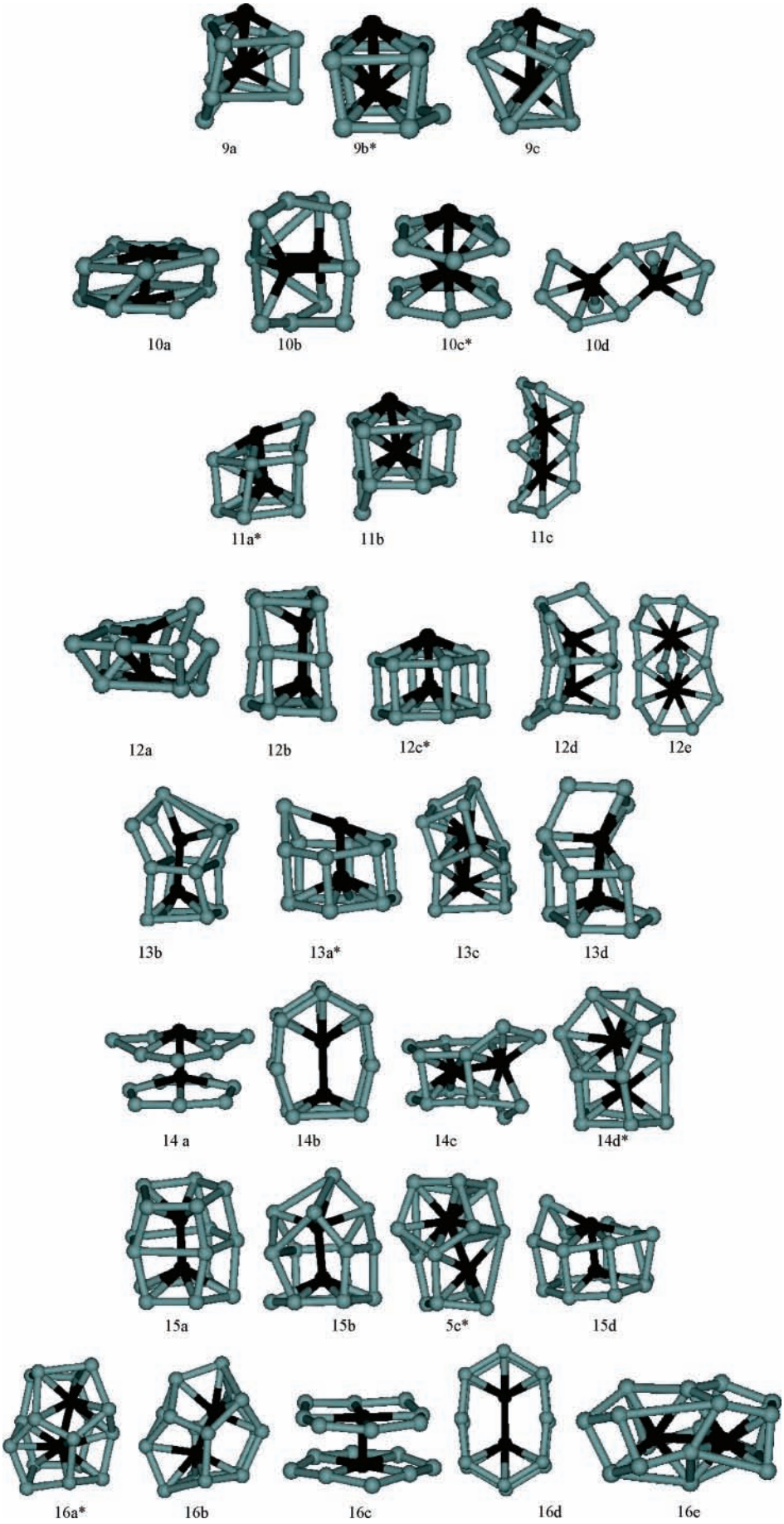

Figure 1. Equilibrium geometries of the Mo_2Si_n ($n = 9-16$) clusters, where the top (or left) Mo atom represents as Mo(1) and the bottom (or right) Mo atom represents Mo(2). Stars indicate the lowest-energy structures of all calculated minima.

TABLE 2: The Calculated Mo−Mo Bond Lengths (Mo−Mo), HOMO, LUMO, HOMO−LUMO Gaps, Total Energies, and Electronic States of the Stable Mo_2Si_n ($n = 9-16$) Clusters

isomer	symmetry	Mo−Mo (Å)	HOMO (hartree)	LUMO (hartree)	HOMO-LU MO (eV)	E_T (hartree)	state
9a	C_1	2.444	−0.2197	−0.1447	2.063	−169.8874176	^{1}A
9b	**C_s**	**2.454**	**−0.2101**	**−0.1531**	**1.566**	**−169.8876134**	**^{1}A′**
9c	Cs	2.954	−0.2175	−0.1322	2.345	−169.8712357	^{1}A′
10a	C_s	2.322	−0.2170	−0.1507	1.826	−173.7254604	^{1}A′
10b	C_s	2.369	−0.2194	−0.1321	2.403	−173.7631692	^{1}A′
10c	**C_1**	**2.457**	**−0.2172**	**−0.1455**	**1.972**	**−173.7934736**	**^{1}A**
10d	C_1	3.179	−0.2154	−0.1491	1.825	−173.7149782	^{1}A
11a	**C_1**	**2.511**	**−0.2165**	**−0.1542**	**1.715**	**−177.6754277**	**^{1}A**
11b	C_1	2.403	−0.2104	−0.1505	1.648	−177.6752242	^{1}A
11c	C_1	2.847	−0.2200	−0.1569	1.737	−177.6138151	^{1}A
12a	C_1	2.514	−0.2151	−0.1522	1.728	−181.513768	^{1}A
12b	C_1	2.493	−0.2264	−0.1575	1.897	−181.527616	^{1}A
12c	**C_1**	**2.355**	**−0.2046**	**−0.1301**	**2.050**	**−181.5801618**	**^{1}A**
12d	C_1	2.644	−0.2196	−0.1581	1.694	−181.5042981	^{1}A
12e	C_1	3.124	−0.2114	−0.1591	1.439	−181.4718664	^{1}A
13a	**C_1**	**2.386**	**−0.2065**	**−0.1456**	**1.675**	**−185.4697197**	**^{1}A**
13b	C_1	2.576	−0.2212	−0.1607	1.665	−185.3869664	^{1}A
13c	C_1	2.673	−0.2169	−0.1648	1.434	−185.4162866	^{1}A
14a	C_1	2.328	−0.1997	−0.1519	1.315	−189.2710007	^{1}A
14b	C_1	2.591	−0.2155	−0.1731	1.165	−189.2686962	^{1}A
14c	C_1	2.656	−0.2206	−0.1606	1.649	−189.2884823	^{1}A
14d	**C_1**	**2.559**	**−0.2228**	**−0.1620**	**1.672**	**−189.3170213**	**^{1}A**
15a	C_1	2.481	−0.2173	−0.1658	1.413	−193.2052867	^{1}A
15b	**C_1**	**2.525**	**−0.2102**	**−0.1558**	**1.494**	**−193.2089852**	**^{1}A**
15c	C_1	2.604	−0.2196	−0.1669	1.450	−193.1906239	^{1}A
15d	C_1	2.352	−0.2084	−0.1518	1.558	−193.1573637	^{1}A
16a	**C_1**	**2.484**	**−0.2212**	**−0.1647**	**1.556**	**−197.1065879**	**^{1}A**
16b	C_{2v}	2.267	−0.2164	−0.1563	1.649	−197.0936387	^{1}A$_1$
16c	C_2	2.204	−0.2214	−0.1250	2.651	−196.9985326	^{1}A
16d	C_1	2.599	−0.2245	−0.1661	1.608	−197.0594728	^{1}A
16e	C_1	3.019	−0.2159	−0.1568	1.625	−197.0315536	^{1}A

2, it is confirmed that the 10d isomer, which is seen as two Si atoms being capped on the planar Mo_2Si_8 frame, is weaker in stability as compared to other stable isomers. Consequently, the 10c isomer is selected as the most stable isomer and the ground state for cluster Mo_2Si_{10}. On the basis of the optimized geometries for the Mo_2Si_n ($n = 9$ and 10) clusters (Figure 1), one can find that the diatomic Mo_2 vertically doped Si_n ($n = 9$ and 10) frame are the dominant growth patterns.

Mo_2Si_{11}. Four possible Mo_2Si_{11} isomers considering various spin configurations are optimized and shown in Figure 1. The 11a and 11b structures, which are generated after one Si atom is surface capped on the 10c isomer, are optimized to be the stable isomers. From the calculated total energies of the 11a and 11b isomers shown in Table 2, the 11a isomer is slightly more stable than the 11b isomer because the total energy of the 11a isomer is a little bit lower than the total energy of the 11b isomer by 0.006 eV. In other words, the 11a and 11b geometries can be seen as the isoenergetic isomers with different geometrical forms. The stable saddle-like 11c isomer is obtained from the 10d geometry, which has a higher total energy comparing with the 11a and 11b isomers. These results reflect that the Mo_2 doped silicon clusters prefer the cagelike structures. Therefore, the opened cagelike geometries are the dominant geometries of the Mo_2Si_{11} isomers.

Mo_2Si_{12}. Guided by the previous theoretical results on the ground state D_{6h} WSi_{12}[25] and Mo_2Si_n ($n = 10$ and 11) clusters described as above, three Mo_2Si_{12} isomers, emerging from one Si atom being surface-capped on the small-sized Mo_2Si_n ($n = 10$, 11) clusters, are obtained and shown in Figure 1. From the findings related to the geometries of the examined systems, the 12a isomer is generated with the serious distortion of the Mo_2 dimer inserted into the irregular hexagonal prism Si_{12} frame with Mo−Mo bond length of 2.514 Å. As for the 12b isomer, it can be described as the Mo_2 dimer being encapsulated into the distorted tetragonal prism D_{4h} Si_{12}. However, from the calculated total energies shown in Table 2, the 12b isomer is more stable than the 12a isomer does. The stable 12c isomer can be seen as one Mo atom being surface capped on the hexagonal prism $MoSi_{12}$ cluster.[3] Furthermore, the 12c isomer is relatively more stable than the 12b isomer because the total energy of 12c isomer is lower by 1.43 eV than that of 12b isomer does (see Table 2). The 12d isomer is seen as an irregular structure and the 12e geometry is obtained with one Si atom being surface-capped on the 11c structure. According to the calculated total energies tabulated in Table 2, it is noticed that the 12e isomer has higher total energy and is less stable than other isomers; consequently, the 12c isomer is the lowest-energy isomer and the ground state for Mo_2Si_{12} cluster. This finding indicates that the Mo_2 doped Si_{12} isomer has the framework that is analogous to the single W atom doped Si_{12} frame.[25]

Mo_2Si_{13}. A variety of possible initial geometries are optimized for the Mo_2Si_{13} cluster and shown in Figure 1. It should be pointed out that the hexagonal prism 13a isomer with one Si atom being parallel surface-capped on the prism Mo_2Si_{12} 12c frame is turned out to be the most stable structure (Table 2). The 13b isomer, which can be described as the distorted prism D_{4h} symmetry, is born after one Si atom is surface capped on the 12b isomer and essentially maintains the analogous framework of the 12b cluster upon adding one silicon atom. The 13c isomer, which is obtained after three Si atoms are surface capped on appropriate sites of the 10c isomer, is optimized to be a stable isomer. However, it is noticed that the 13c and 13b isomers are 1.454 and 2.252 eV higher in total energies than the 13a isomer has, which indicates that the Mo_2 encapsulated Si_{13} frame is not the dominant geometry of the Mo_2Si_{13} clusters. Furthermore, the growth pattern of the small-sized Mo_2 doped Si_n ($n \leq 13$) clusters is similar to that of the Mo doped Si_n frames, and the opened cagelike geometries are the dominant structures.

Mo_2Si_{14}. Starting from various initial structures, the Mo_2Si_{14} cluster is calculated by considering with different spin configurations. Four isomers are identified for the Mo_2Si_{14} cluster, which are the distorted heptagonal prism 14a isomer with Mo_2 dimer acting as the symmetrical axis, the heptagonal prism 14b isomer with Mo_2 dimer vertically to the prism symmetrical axis, the seriously distorted heptagonal prism 14c isomer, and the cagelike C_1 14d isomer, respectively, shown in Figure 1.

Two remarkable Mo_2 encapsulated sandwicklike silicon isomers, namely, 14a and 14b, are formed. The 14a geometry with Mo_2-encapsulated sandwich-like heptagonal prism D_{7h} Si_{14} frame is considered; however, the final optimized geometry reveals that the Mo_2 atoms in the Mo_2Si_{14} isomer move from the center sites of the Si_{14} frame to the each center site of the planar Si_7 unit and the Mo−Mo bond length of the Mo_2 dimer is finally elongated under the interaction between two Si_7 units because the Si−Mo interactions are stronger than the Mo−Mo interaction as mentioned above. However, there is a stable structure where the Mo_2 atoms can be vertically encapsulated into the sandwich-like or boat-like Mo_2Si_{14} 14b geometry with Mo_2 dimer vertically to the symmetrical axis of two Si_7 units. In addition, the 14c isomer is the derivative of the 14b isomer and is more stable than the 14b isomer with the difference of the total energies being 0.538 eV. As observed from the optimized geometries and energies in Table 2, it can be seen that the lowest-energy isomer is a compressed quadrangular prism Mo_2Si_{14} 14d structure, which is described as the Si_2 dimer being surface capped on the top of the slight distorted 12b geometry. Furthermore, the dominant geometries of the Mo_2Si_{14} isomers are the Mo_2 encapsulated Si_{14} structures which are different from the Mo_2 doped cagelike opened Si_n ($n \leq 13$) isomers while the sandwich-like 14a and 14b geometries are not the dominant geometries. Our results show that the Mo_2Si_n ($n \leq 13$) geometries are the cagelike opened isomers while the Mo_2Si_n ($n \geq 14$) geometries are the cagelike closed isomers, and consequently, the structure transition occurs at $n = 14$.

Mo_2Si_{15}. The optimized geometries indicate that the possible Mo_2Si_{15} isomers with high symmetries are not the stable structures. However, after undergoing the slight distortion of the Mo_2Si_{15} geometry to the low symmetry, the stable C_1 15a isomer is finally obtained (Figure 1). The cagelike pentagonal prism 15a isomer is described as the Mo_2 dimer being parallel inserted to the pentagonal Si_{15} frame with Mo−Mo bond length of 2.481 Å, which indicate that the Mo_2Si_{15} geometry is composed of the two sandwich-like $MoSi_{10}$ units and the Mo−Mo bond length in this isomer is longer than that in the free Mo_2 dimer. In this isomer the attractive interactions between each Si_{10} unit and Mo atom are stronger than the interaction between Mo and Mo atoms. It is worth to point out that the 15a and 15b can be seen as the degenerated isomers in energy because from Table 2 the difference of total energies between them is very small. As for as the deformed cagelike 15b and 15c isomers are concerned, the two isomers are described as the diatomic Mo_2 dimer being encapsulated into the Si_{15} frame; furthermore, the 15b cage is more sable than the 15c cage because as shown in Table 2 the total energy of isomer 15b is lower than that of isomer 15c by 0.50 eV. In addition, the 15d isomer is considered, which is generated when one Si atom is surfaced-capped on the heptagonal prism 14a isomer, to form sandwich-like structure. But the sandwich-like 15d isomer is higher in total energy than the 15b and 15c isomers by respective 1.505 and 0.905 eV. Therefore, the stability of Mo_2 doped prismlike Si_{15} geometry is weaker than the Mo_2 encapsulated caged Si_{15} geometry in which the Mo_2 atoms in the cagelike geometries interact with more silicon atoms simultaneously with unequivalent Mo−Si bond lengths and try to terminate the dangling bonds of the silicon atoms with delocalized covalent bonds. Inspection of the calculated total energies of the Mo_2Si_{15} isomers from Table 2, we can find that the 15b isomer is the lowest-energy structure, and corresponds to the ground state of this size ($n = 15$) cluster.

Mo_2Si_{16}. As for as the Mo_2Si_{16} 16a isomer is concerned, the geometry can be described as the Mo_2 dimer being encapsulated into the slight distorted cagelike D_{4d} Si_{16} frame. Furthermore, the doped Mo−Mo bond length in the 16a cluster is 2.484 Å, which is longer than the free quintet diatomic bond length of 2.141 Å with electronic state of $^5\Sigma_g$. Because the attractive interactions between Mo_2 and Si_{16} frame are stronger than that between Mo and Mo atoms, and the Mo_2 dimer is finally dissociated under the attractive interactions of Mo_2 dimer and Si_{16} frame, the formed 16a isomer is composed of the two sandwich-like $MoSi_8$ units. From the calculated total energy for Mo_2Si_{16} isomers in Table 2, obviously, the 16a geometry is the lowest-energy isomer. The C_{2v} Mo_2Si_{16}16b isomer is obtained after the Mo_2 dimer is inserted to the Si surface-capped distorted 15a frame. However, the 16a isomer is more stable than the 16b isomer because as shown in Table 2 the total energy of 16b isomer is higher that that of 16a isomer by 0.352 eV. Guided by above investigations on the 14a and 14b isomers, the striking 16c and 16d isomers are also considered. The C_2 16c isomer is depicted as the Mo_2 isomer being parallel inserted into the octagonal prism Si_{16} frame, in turn, the final obtained 16c geometry is composed of the two planarlike $MoSi_8$ units with electronic state of ^1A; and the Mo−Mo bond length being 2.204 Å which is slightly longer than the free Mo_2 bond length. From Table 2 it can be seen that the 16c isomer is higher in total energy than the 16a and 16b isomers by 2.940 and 2.588 eV respectively. As a consequence, the layered 16c structure is not the most stable building block for the formation of new materials. The 16d isomer is depicted as the Mo_2 isomer being vertically inserted the sandwich-like octagonal prismlike Mo_2Si_{16} structure. Interestingly, this structure is less stable than the 16a isomer and is not selected as the ground state and building block of new material with novel properties. Therefore, the sandwich-like 16c and 16d isomers are not the dominant geometries after examined by the calculated total energies. In addition, the irregular 16e isomer is also considered and optimized as the stable geometry, but its total energy is obviously higher than that of the encapsulated 16a structure has.

According to the above discussions, one can concluded that the stable layered sandwich-like structures are not the most stable structures and cannot be seen as the building block for bulk material and nanotube. As for the most stable bimetal Mo_2 encapsulated silicon clusters, it shows that the opened cagelike Mo_2Si_n ($n \leq 13$) clusters, which are based upon the $MoSi_{10}$ and $MoSi_{12}$ clusters, are the dominant geometries for the middle-sized clusters while the Mo_2 encapsulated silicon clusters are the dominant geometries for the large-sized clusters.

3.2. The Relative Stabilities. In order to investigate the relative stabilities of the most stable Mo_2Si_n ($n = 9-16$) clusters, it is significant to calculate the averaged atomic binding energies for the Mo_2Si_n clusters ($E_b(n)$) and the fragmentation energies ($D(n,n-1)$) with respect to removal of one Si atom from the most stable Mo_2Si_n clusters. The averaged atomic binding energies and fragmentation energies of the Mo_2Si_n ($n = 9-16$) clusters are defined as

$$D(n,n-1) = E_T(Mo_2Si_{n-1}) + E_T(Si) - E_T(Mo_2Si_n)$$

$$E_b(n) = [2E_T(Mo) + nE_T(Si) - E_T(Mo_2Si_n)]/(n+2)$$

where $E_T(Mo_2Si_{n-1})$, $E_T(Si)$, $E_T(Mo)$, and $E_T(Mo_2Si_n)$ denote the total energies of the respective Mo_2Si_{n-1}, Si, Mo, and Mo_2Si_n clusters. The calculated E_b(n) and $D(n,n-1)$ values of the most stable Mo_2Si_n ($n = 9-16$) isomers are plotted as the curves of E_b and $D(n,n-1)$ against the corresponding number of the Si atoms in Figure 2 and Figure 3 and also summarized in Table 3. It should be mentioned that the features of the size-evolution are intuitively viewed and the peaks of the curves correspond to those clusters have enhanced local stabilities.

The averaged atomic binding energies of the Mo_2Si_n clusters are calculated, which are listed in Table 3 and shown in Figure 2. The curve in Figure 2 shows the similar tendency to the calculated fragmentation energies (Figure 3) except for $n = 13$, indicating that the predicted relative stabilities of the Mo_2Si_n vary synchronously with the cluster size.

According to the calculated fragmentation energies shown in Figure 3 and Table 3, two remarkable peaks at $n = 10$ and 12 for the Mo_2Si_n ($n = 9-16$) clusters are found, showing that the corresponding clusters have slightly stronger relative stabilities and have large abundances in mass spectroscopy as compared to the corresponding neighbors. From Figures 2 and Figure 3, the particularly most stabile geometry can be assigned to the cluster of Mo_2Si_{10}, which is slightly higher in fragmentation energy than the Mo_2Si_{12}. Interestingly, these findings of the bimetal Mo_2 doped silicon clusters are slightly different from those of the single TM doped silicon clusters.[31] This finding, underlining once more the prominent role of the Si_{10} matrix, is relevant for the architecture of metal−silicon clusters. It is indicated that the Mo_2Si_{10} cluster is treated more thoroughly in the context of the previous literature on clusters of the form $TMGe_{10}$,[8] since the Mo_2Si_{10} cluster addresses the case of multiple metal impurities. Furthermore, the calculated fragmentation energies in term of the 10c isomer show that it has the strongest stability of all Mo_2Si_{10} isomers, reflecting that the prismlike structures are the preferred geometries. According to the calculated total energies of the Mo_2Si_{15} isomers, it is noticed that the 15a isomer can act as the building block for the novel material because it is the most stable isomer which is composed of two $MoSi_{10}$ 10c units. The calculated ionization potentials (IPs) for the Mo_2Si_n ($n = 12$, 13, and 14) clusters are 6.43, 6.72, and 7.13 eV, respectively. The obtained results reflect that the Mo_2Si_{14} cluster has the strongest chemical stability.

3.3. Population Analysis. The net Mulliken populations (MP) and Natural populations (NP) of the Mo atoms in the most stable Mo_2Si_n isomers are listed in Table 4, the Mo(1) and Mo(2) are defined as in Figure 1, both the MP and NP for the most stable Mo_2Si_n isomers draw the consistent conclusion. The net MP and NP values for the Mo atoms in the Mo_2Si_n ($n = 9-16$) clusters are negative except the MP of the Mo(1) in the 10c isomer (Table 4), showing that the charges in the corresponding clusters transfer from the Mo atoms to the Si_n frames. And the unsaturated d orbitals of Mo atoms obtain the electrons from the Si atoms and S orbitals of Mo atoms, which is also clearly shown in Table 5. These results are coincidence with previous findings on $ReSi_n$ and WSi_{15}.[27,30] As the general trend, the MP as well as 4d orbital populations of Mo(1) and Mo(2) are first increased to some certain values then decreased. However, the NP and 4d orbital populations of Mo(2) atom are gradually increased as the number of Si atoms increasing. Interestingly, the 5s orbital populations of the Mo atoms are independent of the size of the clusters because they vary very small. It should be pointed out that the encapsulated Mo atoms in the most stable Mo_2Si_n ($n = 9-16$) clusters obtain more charges from their surroundings than the surface-capped Mo atoms do, and that the encapsulated Mo atom has a tendency to interact with more silicon atoms with unequivalent bond lengths and try to

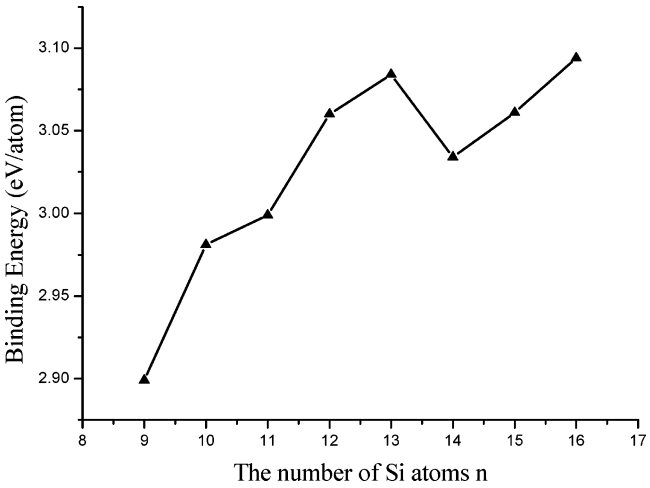

Figure 2. Size dependence of the averaged atomic binding energies of the most stable Mo_2Si_n clusters.

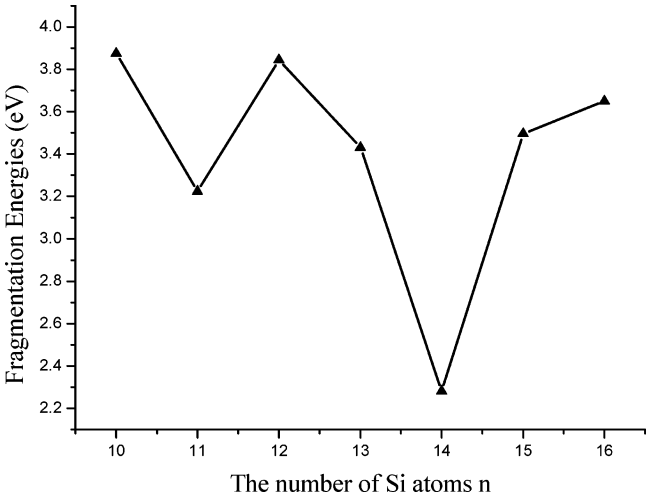

Figure 3. Size dependence of the fragmentation energies of the most stable Mo_2Si_n clusters.

TABLE 3: The Calculated Fragmentation Energies ($D(n,n-1)$) and the Averaged Atomic Binding Energies (E_b) of the Most Stable Mo_2Si_n ($n = 9-16$) Clusters (Unit: eV)

size (n)	9	10	11	12	13	14	15	16
$D(n,n-1)$		3.874	3.224	3.844	3.431	2.281	3.496	3.650
E_b	2.899	2.981	2.999	3.060	3.084	3.034	3.061	3.094

TABLE 4: Mulliken and Natural Populations of the Mo Atoms of the Most Stable Mo_2Si_n ($n = 9-16$) Systems, Where the Mo(1) and Mo(2) Correspond to the Top (or Left) Mo and Bottom (or Right) Mo Atoms in Figure 1

	Mo(1)		Mo(2)	
isomer	MP	NP	MP	NP
9a	−0.869	−0.344	−2.112	−1.437
10c	0.1099	−0.4058	−1.1944	−1.5400
11a	−1.4350	−0.5663	−2.2982	−1.6636
12c	−0.9287	−0.2165	−2.4364	−1.5178
13a	−0.0720	−0.3455	−1.0097	−1.4585
14d	−1.7822	−1.2927	−2.0947	−1.6547
15a	−2.4850	−1.7451	−2.3260	−1.6905
16a	−2.2132	−1.4206	−2.3890	−1.7138

TABLE 5: The Natural Electronic Configurations of the Mo Atoms in the Most Stable Mo_2Si_n ($n = 9-16$) Systems

	Mo(1)		Mo(2)	
isomer	5s	4d	5s	4d
9b	0.30	6.01	0.39	6.89
10c	0.27	6.08	0.40	6.99
11a	0.31	6.18	0.39	7.12
12c	0.19	5.98	0.34	6.97
13a	0.29	5.98	0.33	6.94
14d	0.35	6.82	0.34	7.17
15a	0.35	7.26	0.36	7.19
16a	0.34	6.96	0.32	7.22

terminate the dangling bonds of silicon atoms. Therefore, the doped Mo atoms play very important roles in the stabilities of the Mo_2Si_n ($n = 9-16$) clusters.

3.4. HOMO and LUMO Properties. The HOMO and LUMO energies as well as the corresponding HOMO−LUMO gaps of the Mo_2Si_n clusters are tabulated in Table 1. Based on our calculated results, it can be seen that for the most stable Mo_2Si_n ($n = 9$, 11, 13−16) clusters the HOMO−LUMO gaps are about 1.6 eV while the Mo_2Si_{12} cluster has the biggest gap, which is reflected in Figure 4. In other words, the chemical stability of the Mo_2Si_{12} clusters is stronger as compared with its neighbors, and the Mo_2Si_{12} cluster has enhanced chemical stability. Therefore, Having strong relative stability and chemical stability, the Mo_2Si_{12} cluster can be seen as the most stable building block and can be selected as candidate of novel nanomaterials. As for as the Mo_2Si_{10} cluster is concerned, it is worth to point out that the HOMO−LUMO gap of the Mo_2Si_{10} being 1.972 eV is slightly smaller than that (2.05 eV) of the Mo_2Si_{12} cluster and therefore the Mo_2Si_{12} cluster is slightly stronger in chemical stability than the Mo_2Si_{10} cluster does. Furthermore, we can predict that the HOMO−LUMO gaps for the Mo_2Si_{10} and Mo_2Si_{12} clusters can be detachable experimentally. Consequently, the Mo_2Si_{10} and Mo_2Si_{12} clusters are stable in ionization and dissociation process and contribute to forming the most stable Mo_2-doped silicon nanoclusters, and make them more attractive for the cluster-assembled nanomaterial.

The contour map of the HOMO for the most stable Mo_2Si_{10} isomer is displayed in Figure 5. It can be seen from the Figure 5 that some π-type and σ-type bonds are formed among the Si_n atoms. The encapsulated Mo atom in the Mo_2Si_{10} interacts with 10 silicon atoms simultaneously and terminates the dangling bonds of silicon atoms while the surface capped Mo atom tries to interact with its neighbor silicon atoms with σ-type bonds.

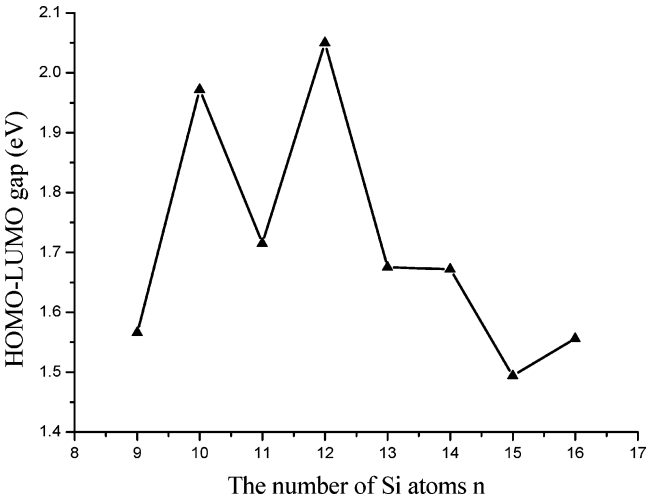

Figure 4. Size dependence of HOMO−LUMO gap of the most stable Mo_2Si_n clusters.

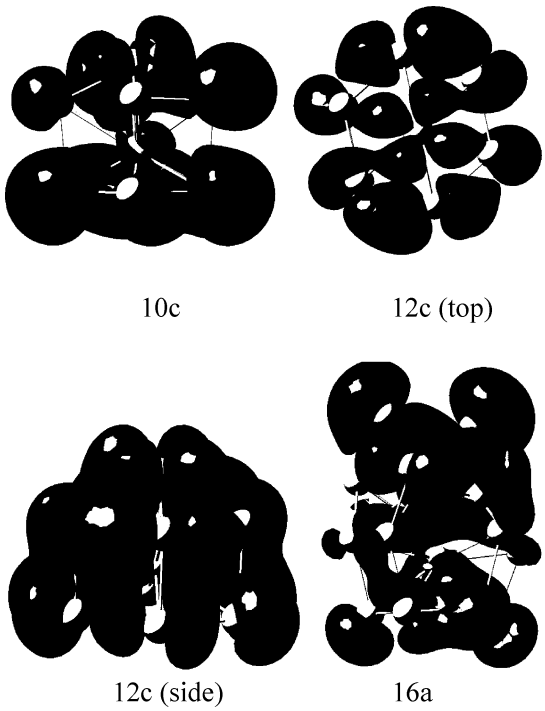

Figure 5. The contour maps of the HOMO for the most stable 10c, 12c, and 16a isomers.

As far as the property of the HOMO of the Mo_2Si_{12} cluster (Figure 5) is concerned, the π-ype bonds are formed among the Si_n atoms, which are distributed beside Mo_2 atoms, and correspond to the delocalized π-type bonds. Furthermore, the encapsulated Mo atom obtains more charges from its bonded silicon atoms and interacts with silicon atoms by relatively weaker d-s σ-type bonds.[3] However, the surface-capped Mo atom have more unfilled d orbitals and try to form the stronger σ-type bonds with its neighbor silicon atoms as compared to the encapsulated Mo atom. From the contour map of the HOMO for the Mo_2Si_{16} cluster shown in Figure 5, it can be obviously seen that each encapsulated Mo atom is surrounded by eight silicon atoms simultaneously, and that the Mo_2 atoms and silicon atoms form the delocalized π-type bonds. Only a few Si−Si bonding contributes to the π-type bonds because the σ-type bonds are the dominant Si−Si bonding type. It should be mentioned that our results show that the Si−Si bonds of the most stable Mo_2Si_{16} cluster is not regular comparing with those Si−Si bonds in the Mo_2Si_{12} cluster.

4. Conclusions

The systematic investigations on the geometrical and electronic properties as well as the growth patterns of the Mo_2Si_n ($n = 9-16$) clusters have been performed theoretically at the (U)B3LYP/LanL2DZ level. All calculated results can be summarized as follows: (1) The most stable Mo_2Si_n clusters in term of the optimized geometries show that the cagelike Mo_2Si_n ($n = 9-16$) clusters are the dominant structures, and within them the Mo atoms prefer to interacting with more silicon atoms. The Mo−Mo distance in these clusters are elongated as compare to the Mo−Mo distance in the free Mo_2 dimer because the Mo−Si interactions are stronger than the Mo−Mo interaction. In the Mo_2Si_n clusters the Si−Si and Mo−Si interactions play more important roles as compared to the Mo−Mo interaction. In other words, the Si−Si and Mo−Si interactions take the dominant effects to the stabilities of the clusters. (2) According to the optimized geometries, the lowest-energy structures feature one

Mo atom inside a Si cage and another one Mo atom on the surface at smaller sizes. As for $n = 14$ and larger, however, both Mo atoms are encapsulated by Si atoms. It is interesting that the Mo_2Si_n clusters undergo a structural transition at $n = 14$. (3) The relative stabilities of the Mo_2Si_n ($n = 9-16$) in term of calculated fragmentation energies are discussed. Our results show that the local maximums of the stabilities of the Mo_2Si_n clusters are the clusters with $n = 10$ and 12, and the Mo_2Si_{10} is the most stable structure. (4) Based upon the calculated natural populations and natural electronic configurations, it is noticed that the charges are transferred from silicon atoms to the 4d orbitals of the Mo_2 atoms. (5) The calculated HOMO and LUMO energies as well as the HOMO−LUMO gaps indicate that the most stable Mo_2Si_{10} and Mo_2Si_{12} clusters have larger HOMO−LUMO gaps and have stronger chemical stabilities as compared to their neighbor size of clusters.

Acknowledgment. This work is supported by National Natural Science Foundation of China (20173055).

References and Notes

(1) Koyasu, K.; Akutsu, M.; Mitsui, M.; Nakajima, A. *J. Am. Chem. Soc.* **2005**, *127*, 4998.
(2) Gueorguiev, G. K.; Pacheco, J. M. *J. Chem. Phys.* **2003**, *119*, 10313.
(3) Wang, J.; Han, J. G. *J. Phys. Chem. A* **2006**, *110*, 12670.
(4) Bloomfield, L. A.; Guesic, M. E.; Freeman, R. R.; Brown, W. L. *Chem. Phys. Lett.* **1985**, *121*, 33.
(5) Harrick, Y. M.; Weltner, W. *J. Chem. Phys.* 1991, *94*, 3371.
(6) Raghavachari, K.; Rohlfing, C. M. *J. Chem. Phys.* **1988**, *89*, 2219.
(7) Li, S.; Weltner, W. R. J.; Raghavachari, K. *Chem. Phys. Lett.* **1995**, *243*, 275.
(8) Wang, J.; Han, J. G. *J. Phys. Chem. B.* **2006**, *110*, 7820.
(9) Kaxiras, E.; Jackson, K.; *Phys. Rev. Lett.* **1993**, *71*, 727.
(10) Majumder, C.; Kulshreshtha, S. K. *Phys. Rev. B* **2004**, *70*, 245426.
(11) Yuan, Z. S.; Tong, X.; Li, W. B.; Liu, X. J.; Xu, K. *THEOCHEM* **2002**, *589*, 229.
(12) Scherer, J. J.; Paul, J. B.; Collier, C. P.; Saykally, R. J. *J. Chem. Phys.* **1995**, *102*, 5190.
(13) Sen, P.; Mitas, L. *Phys. Rev. B* **2003**, *68*, 155404.
(14) Wang, J.; Han, J. G. *J. Chem. Phys.* **2005**, *123*, 244303.
(15) Majumder, C.; Kulshreshtha, S. K. *Phys. Rev. B* **2004**, *69*, 115432.
(16) Jarrold, M. F.; Bower, J. E. *J. Chem. Phys.* **1992**, *96*, 9180.
(17) Menon, M.; Subbaswamy, K. R. *Chem. Phys. Lett.* **1994**, *219*, 219.
(18) Beck, S. K. *J. Chem. Phys.* **1989**, *90*, 6306.
(19) Hiura, H.; Miyazaki, T.; Kanayama, T. *Phys. Rev. Lett.* **2001**, *86*, 1733.
(20) Scherer, J. J.; Pau, B.; Collier, C. P.; Saykally, R. J. *J. Chem. Phys.* **1995**, *103*, 9187.
(21) Zheng, W.; Nilles, J. M.; Radisic, D.; Bowen, K. H. *J. Chem. Phys.* **2005**, *122*, 071101.
(22) Ohara, K.; Miyajima, K.; Pramann, A.; Nakajima, A.; Kaya, K. J. *J. Phys. Chem. A* **2002**, *106*, 3702.
(23) Xiao, C.; Abraham, A.; Quinn, R.; Hagelberg, F.; Lester, W. A. Jr. *J. Phys. Chem. A* **2002**, *106*, 11380.
(24) Wu, Z. J.; Su, Z. M. *J. Chem. Phys.* **2006**, *124*, 184306.
(25) Han, J. G.; Xiao, C.; Hagelberg, F. *Struct. Chem.* **2002**, *13*, 173.
(26) Miyazaki, T.; Hiura, H.; Kanayama, T. *Phys. Rev. B* **2002**, *66*, 121403.
(27) Han, J. G.; Shi, Y. Y. *Chem. Phys.* **2001**, *266*, 33.
(28) Zhao, R. N.; Ren, Z. Y.; Guo, P.; Bai, J. T.; Zhang, C. H.; Han, J. G. *J. Phys. Chem. A* **2006**, *110*, 4071.
(29) Guo, P.; Ren, Z. Y.; Yang, A. P.; Han, J. G.; Bian, J.; Wang, G. H. *J. Phys. Chem. A* 2006, *110*, 7453.
(30) Han, J. G.; Ren, Z. Y.; Lu, B. Z. *J. Phys. Chem. A* **2004**, *108*, 5100.
(31) Wang, J.; Han, J. G. *J. Chem. Phys.* **2005**, *123*, 064306.
(32) Han, J. G.; Hagelberg, F. *Chem. Phys.* **2001**, *263*, 255.
(33) Goicoechea, J. M.; Sevov, S. C. *J. Am. Chem. Soc.* **2006**, *128*, 4155.
(34) Mpourmpakis, G.; Froudakis, G. E.; Andriotis, A. N.; Menon, M.; *Phys. Rev. B* **2003**, *68*, 125407.
(35) Han, J. G. *Chem. Phys.* **2003**, *286*, 181.
(36) Becke, A. D. *Phys. Rev. A* **1988**, *38*, 3098.
(37) Lee, C.; Yang, W.; Parr, R. G. *Phys. Rev. B* **1988**, *27*, 785.
(38) Wadt, W. R.; Hay, R. J. *J. Chem. Phys.* **1985**, *82*, 284.
(39) Frisch, M. J.; Trucks, G. W.; Schlegel, H. B.; Scuseria, G. E.; Robb, M. A.; Cheeseman, J. R.; Montgomery, J. A., Jr.; Vreven, T.; Kudin, K. N.; Burant, J. C.; Millam, J. M.; Iyengar, S. S.; Tomasi, J.; Barone, V.; Mennucci, B.; Cossi, M.; Scalmani, G.; Rega, N.; Petersson, G. A.; Nakatsuji, H.; Hada, M.; Ehara, M.; Toyota, K.; Fukuda, R.; Hasegawa, J.; Ishida, M.; Nakajima, T.; Honda, Y.; Kitao, O.; Nakai, H.; Klene, M.; Li, X.; Knox, J. E.; Hratchian, H. P.; Cross, J. B.; Bakken, V.; Adamo, C.; Jaramillo, J.; Gomperts, R.; Stratmann, R. E.; Yazyev, O.; Austin, A. J.; Cammi, R.; Pomelli, C.; Ochterski, J. W.; Ayala, P. Y.; Morokuma, K.; Voth, G. A.; Salvador, P.; Dannenberg, J. J.; Zakrzewski, V. G.; Dapprich, S.; Daniels, A. D.; Strain, M. C.; Farkas, O.; Malick, D. K.; Rabuck, A. D.; Raghavachari, K.; Foresman, J. B.; Ortiz, J. V.; Cui, Q.; Baboul, A. G.; Clifford, S.; Cioslowski, J.; Stefanov, B. B.; Liu, G.; Liashenko, A.; Piskorz, P.; Komaromi, I.; Martin, R. L.; Fox, D. J.; Keith, T.; Al-Laham, M. A.; Peng, C. Y.; Nanayakkara, A.; Challacombe, M.; Gill, P. M. W.;Johnson, B.; Chen, W.; Wong, M. W.; Gonzalez, C.; Pople, J. A. *Gaussian03*; Gaussian, Inc.: Wallingford, CT, 2004.
(40) Huber, K. P.; Herzberg, G. *Constants of Diatomic Molecules*; New York, 1979.
(41) Chatillon, C.; Aillbert, M.; Pattoret, A. *Acad. Sci. Ser.* **1975**, C *280*, 1505
(42) Honea, E. C.; Ogura, A.; Peale, D. R. *J. Chem. Phys.* **1999**, *110*, 12161.
(43) Huaiming, W.; Craig, R.; Haouari, H.; Dong, J. G.; Hu, Z. D.; Vivoni, A.; Lombardi, J. R.; Lindsay, D. M. *J. Chem. Phys.* **1995**, *103*, 3289.
(44) Delley, B.; Freeman, A.; Ellis, D. E. *Phys. Rev. Lett.* **1983**, *50*, 488.
(45) Morse, M. D. *Chem. Rev.* **1986**, *86*, 1049.